

# Near and mid-IR sub-arcsecond structure of the dusty symbiotic star R Aqr

P.G. Tuthill<sup>1,2</sup>, W.C. Danchi<sup>1</sup>, D.S. Hale<sup>1</sup>, J.D. Monnier<sup>1,3</sup>,

and

C.H. Townes<sup>1</sup>

## ABSTRACT

The results of a high-resolution interferometric campaign targeting the symbiotic long-period variable (LPV) R Aqr are reported. With both near-infrared measurements on baselines out to 10m and mid-infrared data extending to 32m, we have been able to measure the characteristic sizes of regions from the photosphere of the LPV and its extended molecular atmosphere, out to the cooler circumstellar dust shell. The near-infrared data were taken using aperture masking interferometry on the Keck-I telescope and show R Aqr to be partially resolved for wavelengths out to  $2.2\ \mu\text{m}$  but with a marked enlargement, possibly due to molecular opacity, at  $3.1\ \mu\text{m}$ . Mid-infrared interferometric measurements were obtained with the U.C. Berkeley Infrared Spatial Interferometer (ISI) operating at  $11.15\ \mu\text{m}$  from 1992 to 1999. Although this dataset is somewhat heterogeneous with incomplete coverage of the Fourier plane and sampling of the pulsation cycle, clear changes in the mid-infrared brightness distribution were observed, both as a function of position angle on the sky and as a function of pulsation phase. Spherically symmetric radiative transfer calculations of uniform-outflow dust shell models produce brightness distributions and spectra which partially explain the data, however limitations to this approximation are noted. Evidence for significant deviation from circular symmetry was found in the mid-infrared and more tentatively at  $3.08\ \mu\text{m}$  in the near-infrared, however no clear detection of binarity or of non-LPV elements in the symbiotic system is reported.

*Subject headings:* binaries: symbiotic – stars: AGB and post-AGB – circumstellar matter – stars: mass loss – techniques: interferometric – stars-individual: R Aqr

## 1. Introduction

R Aqr is a mass-losing long-period variable (LPV) star believed to be in a symbiotic system with an obscured hot companion whose presence is betrayed by nebular emission lines. Long noted for its peculiar elliptical visible nebulosity extending up to  $2'$  (first reported in Lampland 1923), this star has recently been subject to intense scrutiny with the latest generation of astronomical instrumentation both on the ground and in space. Much of this attention can be traced to the detection in the optical (Wallerstein 1978; Herbig 1980) and radio (Sopka et al. 1982) of what is believed to be the nearest astrophysical jet to

---

<sup>1</sup>Space Sciences Laboratory, University of California, Berkeley, Berkeley, CA 94720-7450, USA

<sup>2</sup>Chatterton Astronomy Department, School of Physics, University of Sydney, NSW 2006, Australia

<sup>3</sup>Smithsonian Astrophysical Observatory, 60 Garden Street, Cambridge, MA, 02138, USA

the earth ( $\sim 200$  pc; Van Leeuwen Feast Whitelock & Yudin 1997; Hollis, Pedelty & Lyon 1997). Thought to originate in the accretion disk around an unseen hot sub-dwarf, this jet has been studied extensively at UV, optical and radio wavelengths (e.g. Burgarella, Vogel & Paresce 1992; Paresce & Hack 1994; Lehto & Johnson 1992).

A difference in location of the peak intensity of the  $\nu = 1, J = 1 - 0$  SiO maser line and the nearby lineless continuum from 7 mm VLA maps was reported by Hollis, Pedelty and Lyon (1997). These authors interpreted the SiO peak as the location of the LPV and the continuum peak marking the accretion disk of the companion, and were thus able to derive a binary separation of  $55 \pm 2$  mas with a position angle of  $18^\circ \pm 2^\circ$ .

With its ability to penetrate layers of obscuring dust, the infrared might be thought an ideal wavelength to image the inner regions of this system, from photospheres of the stars to dust and jets in their immediate surroundings. However the high angular resolutions required and the presence of the enormously luminous LPV have limited the efficacy of this approach. Infrared interferometric measurements with the IOTA array (Van Belle et al. 1996) yielded photospheric diameter measurements of  $\sim 14$ – $15$  mas for the LPV but no evidence for an additional component. Speckle observations at J band (Karovska McCarthy & Christou 1994) suggestive of an elongated image were interpreted in terms of a distorted inner dust shell, possibly due to the presence of the companion. Anandarao & Pottasch (1986) were able to match the near- to far-IR fluxes using a two-temperature dust shell model, while more recently Le Sidaner & Le Bertre (1996) were able to fit similar spectral energy distributions with a simple uniform outflow model.

In the following section of this paper, we briefly describe our observational methods and apparatus for obtaining near- and mid-IR interferometric measurements. In Section 3 the experimental results are given, together with discussion of model fitting and physical interpretation. A brief summary of our conclusions is found in Section 4.

## 2. Observations

A brief synopsis of the observing techniques used to secure the near- and mid-IR interferometric measurements is given below. Near-IR data was taken at the Keck-I telescope in 1998 July and 1999 January covering 4 narrowband wavelengths between 1.25 and 3.08  $\mu\text{m}$ . Visibility data at 11.15  $\mu\text{m}$  were taken with the Infrared Spatial Interferometer (ISI) over the period 1992 to 1999 with various baselines sampling the visibility function.

### 2.1. Near-Infrared Interferometry

Near-IR observations at the Keck-I telescope have utilized the technique of aperture masking interferometry, in which a mask is placed over the telescope pupil so as to only pass light from selected regions, in effect transforming the telescope into an array of small subapertures. Starlight passing through the mask, in this case a 21-hole non-redundant configuration, was brought to a focus in the Near InfraRed Camera (Matthews & Soifer 1994; Matthews et al. 1996), a  $256 \times 256$  InSb array with a pixel scale of 20.57 milli-arcsec/pixel. At focus, an interference pattern is formed containing sets of fringes at various spatial frequencies corresponding to baselines in the pupil. Subsequent analysis of datasets consisting of 100 rapid-exposure ( $\sim 140$  msec) frames using Fourier techniques enables recovery of the visibility

amplitudes and closure phases corresponding to the complex visibility function of the object. With the exception of the sparse telescope pupil which has been shown to confer signal-to-noise advantage for bright targets, the observational and data processing techniques used were very similar to those utilized in speckle interferometry (for a review, see Roddier 1988).

After calibration utilizing nearly-contemporaneous observations of nearby point-source stars, the visibility data could be interpreted in a number of ways, including the fitting of model brightness distributions. The recovery of diffraction-limited maps was also possible with the help of self-calibration methods such as the Maximum-Entropy Method (Gull & Skilling 1984; Sivia 1987) or CLEAN algorithm (Högbom 1974). The signal-to-noise advantages of sparse-aperture observations for bright sources have been exploited previously (e.g., Baldwin et al. 1986; Haniff et al. 1987; Roddier 1988), while a more detailed description of this particular apparatus and technique may be found in Monnier et al. (1999) and Tuthill et al. (1999a). An observing log of near-IR observations is given in Table 1 showing the dates, filters and stellar phases (Mattei 1999) pertaining to our two sets of measurements in 1998 June and 1999 January.

## 2.2. Mid-Infrared Interferometry

Our mid-IR visibility data were obtained at  $11.15\ \mu\text{m}$  with the U.C. Berkeley ISI, a two-element heterodyne stellar interferometer located on Mt. Wilson, CA. Both telescopes are mounted within movable semi-trailers which allowed periodic reconfiguration of the baseline from 4 to 32 m over the course of these measurements. Detailed descriptions of the apparatus and recent upgrades can be found in Bester et al. (1990; 1994), Lipman (1998) and Hale et al. (1999). A journal of R Aqr observations taken with the ISI is provided in Table 2, which shows observations broken into seven separate observing epochs labeled for convenience ‘A’ through ‘G’. As individual visibility measurements taken with the ISI can have low signal-to-noise, we have averaged together measurements taken over these periods with the result that the observing parameters (such as sky position angle or stellar variability phase) pertinent to any single datum can be traced back to the range of values given in Table 2. Observations of K giant stars  $\alpha$  Tau and  $\alpha$  Boo were utilized to monitor system visibility drifts which could be as large as 15% from year to year, thus ensuring reliable calibration (to better than 5%) of science targets as is discussed at some length in Danchi et al. (1990; 1994)

## 3. Results and Discussion

### 3.1. Near-Infrared Visibility Measurements

The principal aim of the near-IR program was to attempt to detect the presence of hot circumstellar material, either in the immediate environment of the LPV or associated with the symbiotic companion. The full two-dimensional Fourier coverage out to 10 m baselines afforded by the masking experiment has proved highly successful at recovering asymmetric circumstellar structures in other systems (e.g., Monnier et al. 1999; Tuthill et al. 1999b). However, in the case of R Aqr, the optical depth to the star is relatively low in the near-IR ( $\tau = 0.01$  at  $2.2\ \mu\text{m}$ ), so that the star greatly outshines the contribution from the dust shell. No circumstellar features were detected at any wavelength in the near-IR from J through K bands, and we are able to place an upper limit of around  $\Delta M \gtrsim 5$  magnitudes for the relative brightness in the near-IR of any such companion.

Table 1. Journal of Near-IR Keck Observations

Date	Filter Wavelength ( $\mu\text{m}$ )	Filter Bandwidth ( $\mu\text{m}$ )	Stellar Phase
1998 Jul 05	1.236	0.011	0.12
1998 Jul 05	1.647	0.018	0.12
1998 Jul 05	2.260	0.053	0.12
1998 Jul 05	3.082	0.101	0.12
1999 Jan 04	2.260	0.053	0.68
1999 Jan 04	3.082	0.101	0.68

Table 2. Journal of Mid-IR ISI Observations

Run Label	Date	Tel Separation (meters)	Spatial Frequency ( $10^5 \text{ rad}^{-1}$ )	Position Angle <sup>a</sup> (Degrees)	Stellar Phase
A	Sep - Oct 92	13.09	7.00 - 11.75	105 - 112	0.68 - 0.74
B <sup>b</sup>	Jun - Jul 94	32.16	16.41 - 28.54	111 - 114	0.36 - 0.39
C	Sep - Oct 94	4.02	1.96 - 3.49	67 - 87	0.61 - 0.68
D	Aug - Sep 97	4.02	1.94 - 3.56	67 - 88	0.37 - 0.40
E	Oct - Nov 97	16.07	8.37 - 14.39	130 - 125	0.50 - 0.58
F	Jul - Aug 98	9.60	2.57 - 8.51	145 - 118	0.24 - 0.29
G	May - Jun 99	4.02	2.14 - 3.47	71 - 87	0.02 - 0.07

<sup>a</sup>Position angle is measured in degrees East of North

<sup>b</sup>One visibility datum at  $28.54 \times 10^5 \text{ rad}^{-1}$  included in this set was taken in Nov 93 at a stellar phase of 0.76

Failure to detect a second star may seem surprising in view of previous indications of a hot companion. Resolution of the interferometry is about 15 mas (FWHM) and the projected distance to a second star might possibly be less than this. However, Hollis et al. (1997) reported indications in 1996 of a companion separated by 55 mas, or 11 AU assuming the distance to R Aqr is 200 pc. The orbital period was estimated to be 44 years, so that its distance during the present measurements would have to be comparable with 55 mas and easily resolved. However, a near-IR intensity less than 1% of that of the R Aqr Mira is in fact not unreasonable. The LPV has a diameter of 15 mas, or 3 AU, whereas a hot star even as large as our Sun would have a diameter at least 100 times smaller, and even allowing for its higher irradiance, a factor of  $\sim 10^3$  less flux should result in the near-IR.

Although the stellar disk of R Aqr itself was not well resolved with the baselines available, its size was determined by fitting the available data. Figure 1 displays visibility curves for four different colors and two observing epochs (see Table 1). In order to increase the signal-to-noise in the plotted data, the two-dimensional visibility function for each wavelength has been azimuthally averaged, allowing visibilities to be plotted as a function of baseline length. On this occasion, additional correction had to be made for the size of the calibrator star 30 Psc, which was itself a late-type (M3III) variable expected from effective temperature and photometric arguments to present an angular diameter of 7.52 mas (Ochsenbein & Halbwachs 1982). Also overplotted on Figure 1 are the best-fitting circular uniform disk model profiles with diameters given in the figure key. As short baseline visibilities can suffer from poor calibration due to seeing changes (the well-known ‘seeing spike’ problem *c.f.* Tuthill et al. 1999a), we have chosen to fit data only at spatial frequencies higher than  $2 \times 10^5 \text{ rad}^{-1}$ .

It should be noted that over the wavelength range  $1.236 - 2.260 \mu\text{m}$  (upper four sets) the stellar diameter is really at the limit of our detection. Visibility curves have only dropped some  $\sim 10 - 20\%$  as compared to an unresolved source. Although the formal diameter errors to the plotted data are small, the larger errors given in Figure 1 reflect systematic sources of uncertainty due to seeing-related mismatches between the source and point calibrator measurements. The likely spread of this dominant term in the uncertainty was determined by examination of large volumes of additional calibration data taken with the same observing parameters. Asymmetries in the errors are a consequence of the nonlinear relationship between visibilities and angular diameters – symmetric error bars on a visibility datum will result in asymmetric diameter errors for such barely-resolved targets. Despite these large uncertainties, we find good agreement with the published K band angular diameters of van Belle et al. (1996) of 14.95 and 14.06 mas in 1995 Jul 11 and 1995 Oct 07. We note also, in passing, that our 1999 January  $2.26 \mu\text{m}$  diameter taken after minimum light is larger than the 1998 June observation near to maximum. Such cycle-dependent size behavior has been studied by Burns et al. (1997) for the case of R Leo, and although our enlargement is in rough accord with this earlier work, our large errors and poor phase sampling cast doubt on the tentative detection of such dynamical changes here.

The masking experiment at the Keck telescope recorded full two-dimensional Fourier information out to the maximum possible  $\sim 10$  m baselines, and in the preceding discussions we have restricted our attention only to the azimuthally averaged visibilities. Departures from circular symmetry would be manifest in the visibilities as a modulation with position angle, while departures from inversion symmetry are indicated by non-zero closure phase signals. As R Aqr is barely resolved, second-order terms in the visibility function were hard to extract given the random and systematic errors on the visibility data. However at all near-IR wavelengths of observation, the visibilities were consistent with a circular disk, with the upper limits on any ellipticity given by the error bars to the circular disk fits given in Figure 1. With the exception of the  $3.08 \mu\text{m}$  observations mentioned below, closure phase signals were within the error bars of zero, implying no

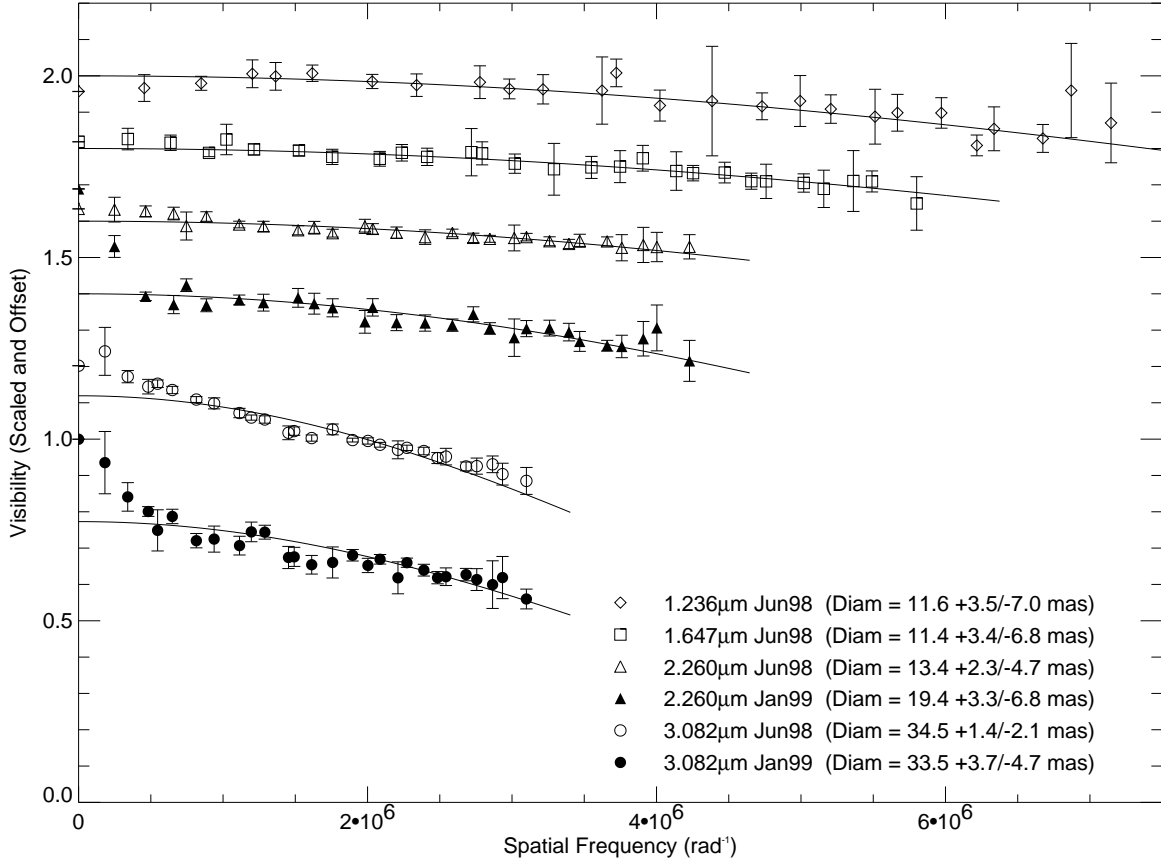


Fig. 1.— Azimuthally averaged visibility data for R Aqr, plotted as a function of spatial frequency, obtained from near-IR observations at the Keck telescope. Open symbols denote data taken on 1998 July 05 (4 colors), while filled symbols show data taken on 1999 January 04 (2 colors). Visibilities have been offset by multiples of 0.2 in order to separate the various datasets on the plot. Overplotted solid lines are best-fitting circular uniform disk model profiles with diameters given in the figure key. These models and the asymmetric errors are further discussed in the text.

significant departures from inversion symmetry in the data.

Images of the R Aqr system in the J band were recently reported by Karovska, McCarthy and Christou (1994) from 1991 November speckle observations with the MMT (effective aperture 6.86 m). These authors found R Aqr to be dramatically elongated, presenting a size of 60 mas along a position angle of  $140^\circ$  while being unresolved in the orthogonal direction. Unfortunately, there is no evidence for such a signal in our data. Our  $1.236 \mu\text{m}$  data rule out elongations greater than 15 mas in any direction, and we note that the expected signal from a 60 mas elongation would cause our Keck visibility function to pass beyond the first null – a radical departure from the observations. Unless profound secular changes in the brightness profile occurred between 1991 and 1999, such elongations appear to be ruled out and we can see of no way to reconcile these two datasets. Full determination of source structure must await the coming generation of separated-element imaging interferometers working at substantially higher angular resolutions.

It is apparent, from Figure 1, that the  $3.08 \mu\text{m}$  data are qualitatively quite different from the shorter wavelength sets, with significantly larger ( $\sim 34$  mas) best-fit uniform disk diameters. Such dramatic enlargement has been reported before, and seems to be most pronounced for objects of extremely late spectral type (Tuthill et al. 1999c). Furthermore, at both 1998 June and 1999 January epochs, the visibilities can be seen to be a poor match to the uniform disk profile, implying instead that a significant proportion of the flux originates in an extended halo. Simple geometrical models, consisting of a uniform disk plus an extended Gaussian shell, were investigated to see if the  $3.08 \mu\text{m}$  visibility functions could be fit. Good fits to both epochs of data were found for models in which  $\sim 20\%$  of the flux came from a Gaussian halo of  $\sim 100$  mas FWHM. Following earlier workers in the optical (Labeyrie et al. 1977; Scholz & Takeda 1987; Haniff, Scholz & Tuthill 1995), changes of angular diameter and radial profile with wavelength can be attributed to the reprocessing of radiation at different levels in the atmosphere by molecular layers whose opacity characteristics are strongly wavelength-dependent. In contrast to the abundance of prominent molecular features such as TiO and VO in optical spectra, recent ISO spectra of a number of late M-type stars (Tsuji et al. 1997) did not show strong spectral structures near  $3.1 \mu\text{m}$ , although there was some unaccounted absorption in this region. Water ice shows an extremely strong absorption at  $3.1 \mu\text{m}$ , however this would seem to be ruled out on physical grounds and further investigation of the possible blanketing effects of common molecules such as CO and  $\text{H}_2\text{O}$  is needed. An alternative scenario is that this extended halo arises from emission from the innermost hot circumstellar dust, just beginning to make its presence felt as we move towards longer wavelength.

As a final note concerning the  $3.08 \mu\text{m}$  data, the closure phase signals did exhibit a small (few degrees) departure from zero as would be expected if the source had a non centro-symmetric brightness distribution. One way the phase signals could be modeled was to allow the  $\sim 100$  mas FWHM Gaussian halo (mentioned above) to move 10 mas to the southwest with respect to the star. Although this identification of non-centro symmetric elements must be labeled as tentative, it is hoped that with the longer baselines available to separated-element interferometers, any such complexity in this source will be subject to careful scrutiny.

### 3.2. Mid-Infrared Visibility Measurements

Visibilities at  $11.15 \mu\text{m}$ , recorded over the seven observing epochs (‘A’ through ‘G’ from Table 2), are plotted in Figure 2. Although an interferometer baseline is a vector quantity, visibilities are shown as a function of the (scalar) baseline length. This approach is often adopted in cases such as this where coverage of the UV plane is sparse so as to make full two-dimensional modeling of the visibility function

unwarranted.

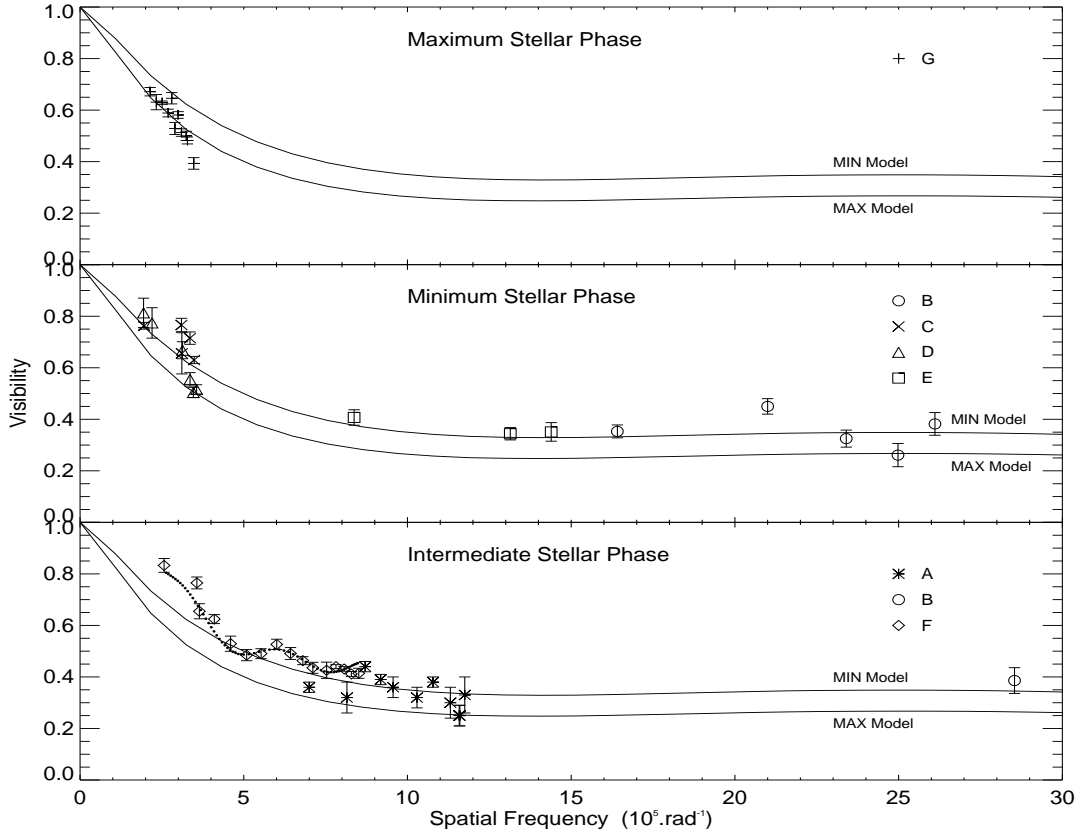


Fig. 2.— Visibility data recorded on R Aqr from observations at the ISI at  $11.15\ \mu\text{m}$ . The topmost panel shows only data taken close to stellar maximum ( $\Delta\Phi \leq \pm 0.125$ ), the second panel shows data close to stellar minimum, while the third panel shows data taken at intermediate stages in the stellar pulsation cycle. The various plotting symbols, identified to the right with the letters ‘A’ through ‘G’, denote different data runs identified in Table 2. Overplotted in each panel are two solid lines showing visibility functions from radiative transfer modeling of the star at stellar maximum and minimum. Also shown on the third (intermediate) dataset is a dotted line showing a model brightness distribution fit to data from set ‘F’ (see text for more details).

Data are separated into three categories according to the stellar phase  $\Phi$  of the LPV at the time of observation (Mattei 1999);  $\Phi > 0.875$  or  $\Phi < 0.125 =$  ‘Maximum’;  $0.375 < \Phi < 0.625 =$  ‘Minimum’; with all other data considered ‘Intermediate’. Although the spatial frequency coverage is far from uniform for all stellar phases, the general shapes of the visibility curves are broadly similar at all phases, and they exhibit two clear components. The relatively rapid drop in visibility at low spatial frequencies argues for a resolved dust shell component, while the flattening off towards high spatial frequencies is indicative of a compact (stellar) component contributing some 30~40% of the flux.



The physical parameters of the R Aqr circumstellar environment were modeled using radiative transfer computations of simulated stellar dust shells attempting to match the visibility data, together with published spectrophotometry. The modeling code used for this purpose, based on the work of Wolfire & Cassinelli (1986), calculates the equilibrium temperature of the dust shell as a function of the distance from the star (assumed to be a blackbody). A wide range of optical properties of dust grains and density distributions of dust shells can be modeled, as is described in more detail in Danchi et al. (1994) and Monnier et al. (1997). As R Aqr has an oxygen-rich atmosphere, it is appropriate to use optical constants for astronomical silicates while the grain size distribution follows that of Mathis, Rumpl & Nordsieck (1977) with dust opacities calculated assuming spheroidal Mie scattering using a method developed by Toon & Ackerman (1981). In the absence of detailed multi-wavelength polarization measurements, this standard model was favored over more complex scenarios such as those with elongated grains, which should have little effect on the main conclusions of the paper except perhaps to produce somewhat different optical depths in model fits. Radiative transfer calculations at 67 wavelengths allow the wavelength-dependent visibility curves, the broadband spectral energy distribution, and the mid-infrared spectrum all to be computed for comparison with observations. Dense sampling of the silicate band in the  $10\ \mu\text{m}$  region is particularly useful for comparison with published spectrophotometry. Figure 3 gives near- and mid-IR spectrophotometric data taken from various literature sources for comparison with model spectra. The optical constants of Draine & Lee (DL 1984), Ossenkopf, Henning, & Mathis (OHM 1992), and David & Papoular (DP 1990), were all tested in modeling the dust shell, with the result that OHM (used hereafter) and DP constants both provided high-quality fits to the shape of the silicate feature, while DL optical constants were not preferred.

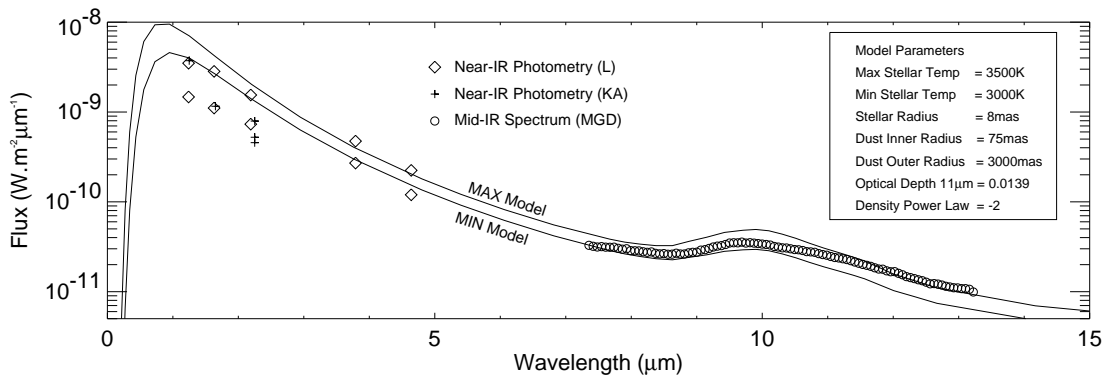


Fig. 3.— Spectral energy distribution of R Aqr. The mid-IR spectrum from Monnier et al. (MGD 1998) was taken at a stellar phase of 0.46. The near-IR points of Le Bertre (L 1993) show points at maximum and minimum light taken from best fits to the near-IR lightcurve from photometric monitoring data. The points of Kamath & Ashok (KA 1999) were all taken fairly close to stellar maximum (0.85  $\sim$  0.99). Overplotted solid lines show numerically computed spectral energy distributions of radiative transfer models at maximum and minimum light. The parameters of these models are given in the box to the right.

For model calculations, the simplifying assumption of uniform isotropic outflow has been made, resulting in a spherical dust shell with a  $\rho \propto r^{-2}$  density distribution beginning at a discrete dust condensation radius. Although there is considerable evidence for departures from spherical symmetry at larger scales, the primary constraints on the models from the mid-IR visibilities and spectra were not

extensive enough to warrant more complex models.

Two models were constructed, one at stellar maximum and one at minimum and their computed mid-IR visibility functions are given in Figure 2, while simulated spectra and physical parameters are in Figure 3. The diameter of the central star was fixed at 16 mas (or 3.2 AU assuming a distance of 200 pc) from near-IR observations (Section 3.1; Van Belle et al. 1996) and the temperature fixed to match the mid-IR luminosity. As can be seen from Figure 2, the visibility data at maximum and minimum light are well fit by the model curves, and we note that all parameters of the dust shell model are identical for the two models, with the increase in stellar flux being simulated by an elevation in the effective stellar temperature of the star by 500 K. This in turn leads to an elevation of the temperature of the dust at the inner radius from 850 K to 1170 K.

Serious inadequacies in this simplest-case model scenario are revealed upon comparison of model predictions with spectro-photometry and intermediate-phase visibility data. As can be seen from Figure 3, the simulated spectral energy distributions are not well matched to the observations. In the mid-IR, although the overall flux level and the shape of the model silicate feature are in fair accord with the measurements of Monnier et al. (1998), the spectral slope towards longer wavelengths is too steep. This lack of long-wavelength flux argues for the presence of more cool dust, or a cooler underlying stellar spectrum. Near-IR photometric measurements (Le Bertre 1993; Kamath & Ashok 1999) fall well below the models implying increased near-IR opacity, or again a cooler underlying star; our model overestimates the bolometric luminosity. However, such decreases in stellar temperature and increases in density of the circumstellar dust shell were not possible without seriously perturbing the fits to the visibility data, in particular the relatively high visibilities recorded at long baselines.

Put simply, the strong point-source (30~40%) evident from the mid-IR visibility curves drives models to low optical depths and in turn high stellar luminosities to account for the mid-IR flux (which could otherwise come from the dust if the optical depth were higher). Although a wide range of model parameter space was explored, including variations on the density-radius law, the inner and outer radii, the dust opacity properties, and the dust densities, no spherically symmetric model could be found which overcame the shortcomings with the spectral fitting. The reader is therefore cautioned against taking the model parameters from Figure 3 as an accurate description of this star; rather they describe the best fit to our interferometric dataset which can be provided by a uniform-outflow spherical dust shell.

There are many imperfections in the modeling process, mostly due to oversimplifications or limited knowledge, which could lead to misfitting of the data. Although the use of a blackbody spectrum for the star is common practice, evolved stars exhibit significant departures (see for example, Lobel Doyle & Bagnulo 1999). The optical properties of the dust can also have a significant impact on the radiative transfer results, and detailed knowledge of crucial aspects such as the true grain size distribution are lacking (the dust of Mathis, Rumpl & Nordsieck 1977 is more appropriate for the ISM). However, it may be that not all difficulties in fitting may stem from the fact that the simple dust radiative transfer models, with available silicate opacity functions do not give a realistic picture of actual circumstellar dust shells.

Examination of the intermediate-phase visibilities (bottom panel, Figure 2) points to an additional possible explanation for the poor spectral performance of our models. While visibilities from data set ‘A’ fall between the Max and Min model curves as might be expected, those from data set ‘F’ are higher than either, especially at low spatial frequencies well covered in the other plots. A likely explanation for this change in visibility can be found by examination of Table 2: most of the short baseline data underpinning the models (sets ‘C’, ‘D’ and ‘G’) along with set ‘A’ were taken at a position angle on the sky of around

$70 \sim 100^\circ$ , while the baselines constituting data set ‘F’ were taken at a very different orientation ( $145^\circ$  for the short-baselines). Hence the difference in these visibilities taken at angles differing by  $45 \sim 75^\circ$  argues for substantial departures from sphericity. In such an anisotropic circumstellar environment, the spherical model assumptions break down and failure to fit to the spectral energy distribution may be the result of complications such as patchy extinction of the star or radiation leaking through holes in the cloud. Indeed, the extension of asymmetric structure from the well-known nebula down to successively smaller scales is not surprising, and has already been suggested from findings of time-variable polarization (Deshpande et al. 1987).

The visibility data set ‘F’ has rather dense sampling over a range of spatial frequencies together with small probable errors, and as is seen from Figure 2, it exhibits wiggles or bumps (e.g. at  $6 \times 10^5 \text{ rad}^{-1}$ ) which indicate departure from a simple smooth radial intensity distribution. In order to assess this further evidence for anisotropy in the R Aqr dust shell, model brightness distributions (not, in this case, based on radiative transfer computations) have been fit, the result of which is overplotted as a dotted line in panel 3 of Figure 2. The stellar component of our best-fit model contributed 36% of the flux, with 61% coming from a spherical circumstellar dust shell assumed to have a simple Gaussian profile with a FWHM of 350 mas. A third component, modeled as a localized point-source contributing 3% of the total flux and located 700 mas from the star at a position angle of  $100^\circ$  (or  $-80^\circ$ ), produces the wiggles noted in the data. Although such a feature might be some localized concentration of dust, or possibly a local warming, serious discussion should be deferred until more complete Fourier coverage can be obtained. With the sparse coverage afforded by the single interferometer baseline, a host of different models could be devised in which some additional flux is originating at some distance from the star and thereby generating the high-frequency signal we see. Therefore the likely significance to be placed upon our model parameters is low. This discussion is included simply as additional evidence for departure from a uniform outflow, and as an encouragement to further efforts at full high angular resolution imaging of this system in the mid-IR.

When non-spherical dust halos occur, it is rarely possible to discriminate between a number of viable outflow models when only relatively limited Fourier data are available, even though reasonable models may be chosen (e.g. Lopez et al. 1997). The simple isotropic outflow model given here provides a reasonable fit to most of our mid-IR visibility data. However, deviations from the model are clear, and the more involved task of mapping and fitting of spectral data await the recovery of the full two-dimensional complex visibility function. For this reason, a detailed comparison with other models such as the two-shell model of Anandarao & Pottasch (1986) or the uniform outflow model of Le Sidaner & Le Bertre (1996) is not given here. However, our inner dust shell radius is in agreement with results of these earlier workers (for Anandarao & Pottasch 1986, we consider only their hot inner shell which should dominate over the cool outer shell ( $T_2 = 87.1 \text{ K}$ ) in this wavelength region). On the other hand, significant differences include lower optical depths and hotter stellar temperatures.

All spherically symmetric models investigated have been found to be inadequate in fitting the expanded dataset encompassing near- and mid-IR interferometry and the spectral energy distribution from the near- to the far-IR. This finding is in agreement with studies of *o* Ceti, another symbiotic system observed interferometrically in the mid-IR Lopez et al. 1997. With further work at high resolutions, particularly directed towards full imaging of these systems, the effects of the companion’s presence, both gravitational and radiative, in the shaping of the circumstellar dust shell may be elucidated.

#### 4. Conclusions

High-resolution interferometric studies of R Aqr at narrow bandwidths within the J, H and K bands find no evidence for any significant departure from the best-fitting model of a marginally-resolved stellar disk, which we identify with the LPV component of the system. Any companion present and separated by more than  $\sim 15$  mas must exhibit a magnitude difference in excess of  $\Delta M \gtrsim 5$  mag in the near infrared. These results are consistent with those of Van Belle et al. (1996), but not with Karovska et al. (1994). An enlargement, by approximately a factor of 2, is reported for the apparent size at a wavelength of  $3.08 \mu\text{m}$  as compared with shorter near-infrared bands, which is attributed to molecular blanketing by an unidentified species in the atmosphere, or thermal emission from material in an extended halo. Tentative evidence for asymmetry at this wavelength is also reported. In the mid-IR, visibility data obtained with the ISI have been used to constrain simple uniform spherical outflow models. Using self-consistent radiative transfer calculations, good fits to most of the visibility data have been obtained. However, serious shortcomings were found when comparing the synthetic spectral energy distributions to measurements, many of which may be attributed to inadequate knowledge of the detailed dust shell parameters. Furthermore, mid-IR interferometry obtained at a different position angle on the sky points towards substantial departures both from spherical symmetry and from a simple radial distribution. These indicate that the shortcomings of the present models are probably in large part be due to the oversimplistic assumption of an isotropic uniform outflow. Further high-resolution studies, both in near-infrared with higher spatial resolution and dynamic range, and in the mid-infrared with more complete Fourier coverage, are important in order to fill in the gaps in understanding of this star.

We thank Everett Lipman for help in securing many of the ISI measurements published herein, and for developmental work on the instrument. Long-baseline interferometry in the mid-infrared at U.C. Berkeley is supported by the National Science Foundation (Grants AST-9315485, AST-9321289, AST-9500525, & AST-9731625) and by the Office of Naval Research (OCNR N00014-89-J-1583 & FDN0014-96-1-0737). Some of the measurements herein were obtained at the W.M. Keck Observatory, made possible by the generous support of the W.M. Keck Foundation, and operated as a scientific partnership among the California Institute of Technology, the University of California, and NASA.

#### REFERENCES

- Anandarao, B. G., & Pottasch, S. R. 1986 *A&A*, 162, 167
- Baldwin, J. E., Haniff, C. A., Mackay, C. D., & Warnier, P. J. 1986, *Nature*, 320, 595
- Bester, M., Danchi, W. C., & Townes, C. H. 1990, in *Amplitude and Intensity Spatial Interferometry*, ed. J. B. Breckinridge, *Proc. SPIE* 1237, 40
- Bester, M., Danchi, W. C., Degiacomi, C. G., & Bratt, P. R. 1994, in *Amplitude and Intensity Interferometry II*, ed. J. B. Breckinridge, *Proc. SPIE* 2200, 274
- Burgarella, D., Vogel, M., & Paresce, F. 1992, *A&A*, 262, 83
- Danchi, W. C., Bester, M., Degiacomi, C. G., & Townes, C. H. 1990, *ApJ*, 359, L59
- Danchi, W. C., Bester, M., Degiacomi, C. G., Greenhill, L. J., & Townes, C. H. 1994, *AJ*, 107, 1469

- David, P., & Papoular, R. 1990, *A&A*, 237, 425
- Deshpande, M. R., Joshi, U. C., Kulshrestha, A. K., Sen, A. K., Rao, N. K. & Raveendran, A. V. 1987, *PASP*, 99, 62
- Draine, B. T., & Lee, H. M. 1984, *ApJ*, 285, 89
- Gull, S. F., & Skilling, J. 1984, *IEEE Proceedings*, 131, Pt. F, No. 6
- Hale, D. D. S., Bester, M., Danchi, W. C., Fitelson, W., Hoss, S., Lipman, E. A., Monnier, J. D., Tuthill, P. G., & Townes, C. H. 1994, in preparation
- Haniff, C. A., Mackay, C. D., Titterington, D. J., Sivia, D., Baldwin, J. E., & Warner, P. J. 1987, *Nature*, 328, 694
- Haniff, C. A., Scholz, M., & Tuthill, P. G. 1995 *MNRAS*, 276, 640
- Herbig, G. H. 1980, *IAU Circ.*, 3535, 2
- Högbom, J. 1974, *ApJS*, 15, 417
- Lehto, H. J. & Johnson, D. R. H. 1992, *Nature*, 355, 705
- Hollis, J. M., Pedelty, J. A., & Lyon, R. G. 1997, *ApJ*, 482, L85
- Kamath, U. S., & Ashok, N. M. 1999, *A&AS*, 135, 199
- Karovska, M., McCarthy, D. W., & Christou, J. C. 1994, *ASP Conf. Ser.* 64: Eighth Cambridge Workshop on Cool Stars, Stellar Systems, and the Sun, 8, 652
- Labeyrie, A., Koechlin, L., Bonneau, D., Blazit, A., Foy, R. 1977, *ApJ*, 218, L75
- Lampland C. O. 1923, *Publ. AAS*, 4, 319
- Le Bertre, T. 1993, *A&AS*, 97, 729
- Le Sidaner, P., & Le Bertre, T. 1996, *A&A*, 314, 896
- Lipman, E. A., 1998, University of California at Berkeley, PhD Dissertation
- Lobel, A., Doyle, J. G. & Bagnulo, S. 1999, *A&A*, 343, 466
- Lopez, B., Danchi, W. C., Bester, M., Hale D. D. S., Lipman, E., Monnier, J. D., Tuthill, P. G., Townes, C. H., Degiacomi, C. G., Gegalle, T. R., Greenhill, L. J., Cruzalébes, P., Lefèvre, J., Mékarnia, D., Mattei, J. A., Nishimoto, D., & Kervin, P. W. 1997, *ApJ*, 488, 807.
- Mathis, J. S., Rumpl, W., & Nordsieck, K. H. 1977, *ApJ*, 217, 425
- Mattei, J. A. 1999, *Private Communication*
- Matthews, K., & Soifer, B. T. 1994, *Infrared Astronomy with Arrays: the Next Generation*, I. McLean ed. (Dordrecht: Kluwer Academic Publishers), p.239
- Matthews, K., Ghez, A. M., Weinberger, A. J., & Neugebauer, G. 1996, *PASP*, 108, 615
- Monnier, J. D., Tuthill, P. G., Lopez, B., Cruzalébes, P., Danchi, W. C., & Haniff, C. A. 1999 *ApJ*, 512, 351

- Monnier, J. D., Geballe, T. R., & Danchi, W. C. 1998, ApJ, 502, 833
- Monnier, J. D., Bester, M., Danchi, W. C., Johnson, M., Lipman, E., Townes, C. H., Tuthill, P. G., Gegalle, T. R., Nishimoto, D., & Kervin, P. W. 1997 ApJ, 481, 420
- Ochsenbein, F., & Halbwachs, J. L. 1982, A&AS, 47, 523
- Ossenkopf, V., Henning, T., & Mathis, J. S. 1992, A&A, 261, 567
- Paresce, F., & Hack, W. 1994, A&A, 287, 154
- Roddier, F. 1988, *Physics Reports*, 170, 97
- Scholz, M., & Takeda, Y., 1987, A&A, 196, 342
- Sivia, D. S. 1987, Cambridge University, PhD Dissertation
- Sopka, R. J., Herbig, G., Michalitsianos, A. G., & Kafatos, M. 1982 ApJ, 258, L35
- Toon, O. B., & Ackerman, T. P. 1981, Appl. Opt., 20, 3657
- Tsuji, T., Ohnaka, K., Aoki, W. & Yamamura, I. 1997, A&A, 320, L1
- Tuthill, P., Monnier, J. D., Haniff, C. A., & Danchi, W. C. 1999a, in preparation
- Tuthill, P.G., Monnier, J.D., & Danchi, W.C. 1999b, Nature, 398, 487
- Tuthill, P.G., Monnier, J.D., & Danchi, W.C. 1999c, in ASP Conf Series *Working on the Fringe: an international conference on optical and IR interferometry from the ground and space* In Press
- Van Belle, G. T., Dyck, H. M., Benson, J. A., & Lacasse, M. G. 1996, AJ, 112, 2147
- Van Leeuwen, F., Feast, M. W., Whitelock, P. A. & Yudin, B. 1997, MNRAS, 287, 955
- Wallerstein, G., & Greenstein, J. L. 1980, PASP, 92, 275
- Wolfire, M. G., & Cassinelli, J. P. 1986, ApJ, 310, 207